Effect of Hf incorporation in solution-processed NiO_x based resistive random access memory

Doo Hyun Yoon, Si Joon Kim, Joohye Jung, Seung Jin Heo, and Hyun Jae Kim[a)]
School of Electrical and Electronic Engineering, Yonsei University, Seoul 120-749, South Korea

(Received 11 December 2013; accepted 7 February 2014; published online 4 March 2014)

Resistive random access memory based on transition metal oxide materials has attracted much recent attention for the development of next-generation non-volatile memory. The Hf:NiO_x devices showed driving mode transformation by the Hf content in the system. Unipolar resistive switching was observed at 2% of Hf concentration while a bipolar resistive switching was observed at 10%. Un-stable switching was shown at 30%, and non-stable breakdown was followed by 100%. These variations of I–V characteristics can enhance understanding of resistive switching phenomenon under the material incorporated system. © *2014 AIP Publishing LLC*.
[http://dx.doi.org/10.1063/1.4867233]

With scaling of semiconductor device technologies into the sub-22-nm generation of non-volatile memory, concerns related to fundamental physical limitations have become more pressing. These fundamental limitations may result in a new paradigm, with radical changes in fabrication processes and materials. One of the more promising alternatives is resistive random-access memory (RRAM) based on transition metal oxides (TMOs), which has attracted significant interest because of the ease of high-density design, reduced-power consumption, short SET/RESET times, and large window of high/low resistance ratios with non-volatile properties.[1–3] Resistivity-switching phenomenon was first reported in 1962, and since then, there have been numerous investigations into this material system.[3] The resistive switching in TMO facilitates a transition between two bi-stable states: a high-resistance state (HRS) and a low-resistance state (LRS). The SET and RESET processes occur via changes in an applied voltage. TMO-based RRAM has two modes of operation, so-called unipolar resistive switching (URS) and bipolar resistive switching (BRS), and different models are used to explain the physical processes that occur in each mode. URS is generally modeled by considering a filament-dominant effect in the oxide films and can be understood in the framework of the thermochemical memory (TCM) model.[3] However, the BRS mode is typically modeled as a combination of filament conduction and interface effects, which are controlled by applying a voltage with the opposite polarity. Generally, the valence-changing memory (VCM) model is most widely used to describe the BRS mode.[3]

Among the various materials, NiO_x has been intensively studied because of the simple constituents and high LRS/HRS ratio ($>10^4$).[4,5] Earlier, intentionally non-stoichiometric NiO_x systems incorporating elements including Ti,[6] Cu,[7] Nb,[8] and Li[9] have been studied. Doping with Ti leads to the creation of metallic Ni defects even at high oxygen pressures, which facilitates bi-stable resistive switching.[6] Similar properties have been observed by doping with Cu and Nb, leading to an improvement in the difference between the switching biases and a reduction of the operating voltage by creation of metallic defects and V_O centers.[7,8] Uniquely, Li incorporation results in an accompanying decrease of the LRS/HRS ratio and an improvement of the thermal stability of the HRS in NiO_x. Furthermore, the prospect of mono-stable threshold switching is more likely with Li doping, which implies that the Li atoms act as oxygen suppliers rather than defect creators.[9] Perceived from abovementioned works, we focused on Hf incorporation and its affection on the variation of the resistive-switching characteristics. Hf has a standard electrode potential (SEP) of −1.70 V, which reflects a tendency toward metal oxidation and is larger than that of the defect-creating elements (Ti: −1.63 V, Cu: +0.15 V, and Nb: −1.09 V) but smaller than that of the oxygen supplier, Li, which has an SEP of −3.04 V. This suggests that both phenomena may be possible through a reduced V_O formation energy, E^f_v, and enhanced oxygen concentration, by optimizing the Hf concentration.[10–12]

The devices were formed from a Pt/Ti/SiO_2/Si substrate. Solution processing was used to form the Hf:NiO_x layers. The precursor solution was synthesized by dissolving Ni nitrate hexahydrate in 2-methoxyethanol with 0.5 M mono-ethanolamine and 0.5 M acetic-acid. Hf chloride hydrate was used in the following compositions: 1:0.02, 1:0.1, 1:0.3, and 1:1 in order to generate 2%, 10%, 30%, and 100% Hf incorporation levels, respectively. A multi-stacking fabrication method, performed with seven sequential spin-coating steps following an initial 20-min 300 °C pre-anneal, was used to enhance the thin-film quality. A post annealing was carried out at 450 °C for 2 h. The thickness of all Hf:NiO_x layers is ∼100 nm. A 100-nm-thick Al was deposited using thermal evaporator.

Figure 1 shows the current-voltage (*I-V*) characteristics of the Al/Hf:NiO_x/Pt device after forming process. The 2% Hf:NiO_x (Fig. 1(a)) thin film displays typical characteristic as pristine NiO_x based device of our previous report.[13] As the applied voltage increased to ∼2.25 V and ∼5.95 V, the RESET and SET process were observed, respectively. Overall, the 2% Hf:NiO_x thin film showed clear switching characteristics, maintaining a high LRS/HRS ratio of $\sim 10^5$. This implies that the incorporated Hf atoms act as defect creators at 2%, and oxygen supply behavior was insignificant.[6–8] When Hf was added up to 10%, the driving mode was changed to BRS

a)E-mail: hjk3@yonsei.ac.kr

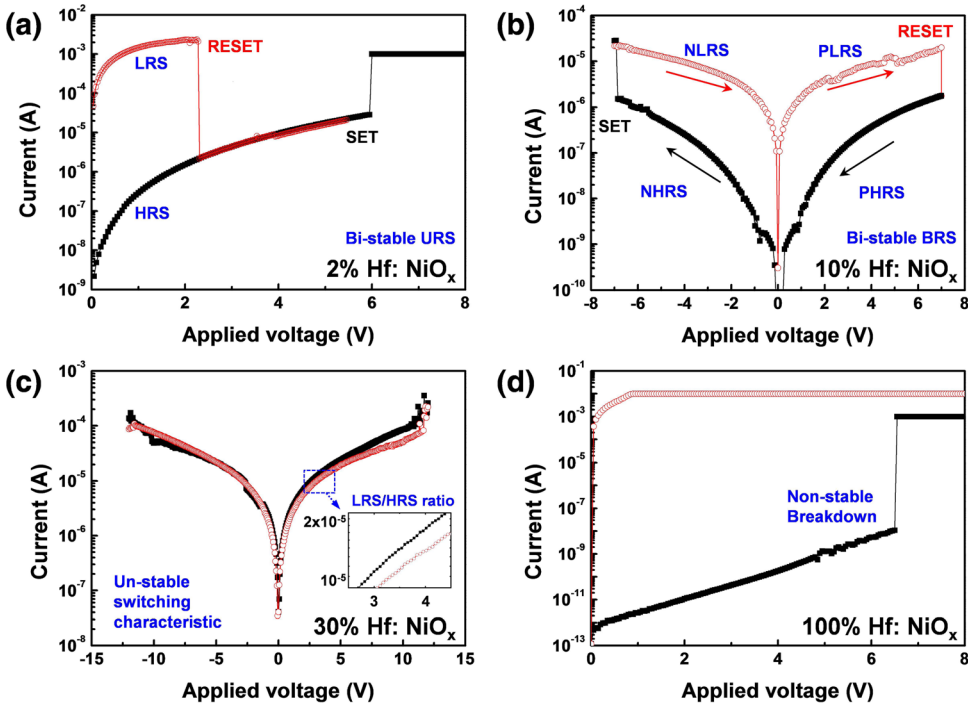

FIG. 1. $I-V$ curves corresponding to the 2%, 10%, 30%, and 100% Hf:NiO_x devices. (a) 2%, bi-stable URS, (b) 10%, bi-stable BRS, (c) 30%, un-stable BRS, and (d) 100%, non-stable breakdown.

mode, as shown in Fig. 1(b). This phenomenon is noteworthy because the transition from bi-stable resistive switching to mono-stable switching has been widely reported in terms of oxygen concentration.[14,15] However, this transformation of resistive-switching modes, from URS to BRS, is rarely observed except in compliance current adjustments,[16] due to the distinctive operation mechanism of each mode. The 10% Hf:NiO_x thin film had a large LRS/HRS ratio of $\sim 10^3$. The SET process was observed at -6.81 V, switching in the negative region of the HRS (NHRS) to the negative region of LRS (NLRS). The RESET voltage of the LRS (PLRS) switching to the positive region of the HRS (PHRS) was $+6.37$ V. The measured RESET current was approximately 0.02 mA, which is 100 times smaller than that of the unipolar switching current observed in the 10% Hf:NiO_x thin film. Figure 1(c) shows the $I-V$ characteristics of the 30% Hf composition thin films. Switching failure was observed, with a degradation of the LRS/HRS ratio to less than a factor of ten. Figure 1(d) shows the $I-V$ characteristics of the 100% Hf:NiO_x device. Non-stable insulator breakdown with permanent short current was observed.

To verify the crystallographic structure of 2%, 10%, 30%, and 100% Hf:NiO_x thin films, we measured X-ray diffraction (XRD) (see supplementary material for Figure S1[24]). As the Hf content increased, the NiO (111), NiO (200), and NiO (220) peaks started to diminish, finally resulting in an amorphous structure. This deteriorated crystallinity is attributed to the non-lattice oxygen component which enlarges the lattice constant and the induced lattice stress owing to the ionic radii difference between Ni to Hf atom.[17] As the grain boundaries are known as the preference site for conduction filament (CF) formation,[18] totally amorphized phase of 100% Hf:NiO_x intimates the permanent breakdown of TMO layer with their non-stable *I-V* characteristics.

Isothermal $I-V$ profiles were used to analyze the transformation between the two bi-stable memory-switching modes, URS and BRS. Figures 2(a) and 2(b) show linear regressions to the $I-V$ curves for 2% and 10% Hf:NiO_x devices in the high-voltage region of HRS, respectively. In both plots, Poole–Frenkel (PF) emission was observed, with a gradient of 1.97 and 2.41, respectively. In contrast to the charge-transport mechanism in the HRS, which follows PF emission for both 2% and 10% Hf:NiO_x, a significant distinction between these two devices was observed at LRS currents. The LRS current of the 2% Hf:NiO_x device showed Ohmic $I-V$ characteristics at voltages smaller than that corresponding to the RESET process, as shown in Fig. 2(c). As the RESET bias was approached in the 2% Hf:NiO_x device, there was a reduction in the gradient of the $I-V$ curve, which implies the formation of metallic CFs, formed from Ni. Thus, the conventional TCM model is applicable to the URS operation mechanism in the 2% Hf:NiO_x device, as shown in Fig. 3(a). Following the initial forming process, the current can flow within the newly formed CFs (LRS) which is mainly composed of metallic Ni. Induced joule heating becomes significant in the metallic Ni path as the injected current density increases. When the applied voltage becomes large enough to cause thermochemical reactions between metallic Ni and oxygen ions, the NiO_x can be formed, which ruptures the filament path (RESET, HRS). This phenomenon is possible due to the preference of lower valence states at high temperatures, which is typical for stable oxide associated with the negative free energy of formation.[3] The reversible transition HRS to LRS (SET) can be possible by higher field injection (over SET voltage), which regenerate the CF again and complete the 1 cycle of memory operation. In contrast to the 2% Hf devices, the LRS $I-V$ characteristic was Ohmic in the 10% Hf:NiO_x devices only at relatively low

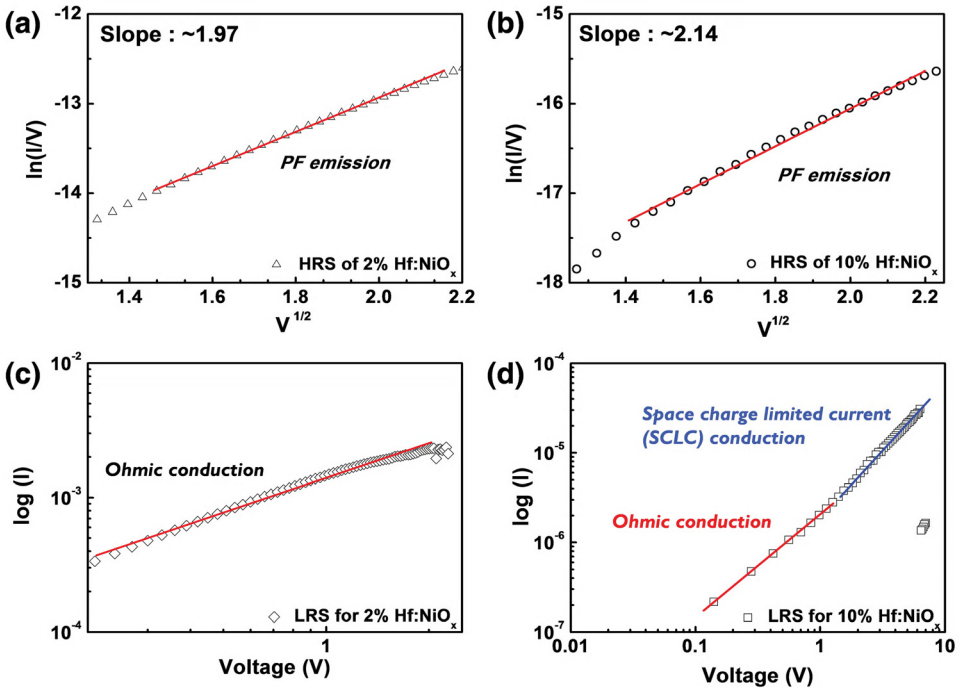

FIG. 2. The HRS $I-V$ characteristics of (a) 2% and (b) 10% Hf:NiO_x. In both cases, PF emission was dominant. (c) LRS $\log(I)-\log(V)$ plot for the 2% indicates Ohmic conduction. (d) LRS $\log(I)-\log(V)$ plot for the 10% shows a transition from un-filled trap SCLC (at low-voltage region) to trap-filled SCLC (at high-voltage region).

voltages, while space-charge limited conduction (SCLC) becomes dominant in the high-voltage region, as shown in Fig. 2(d). This Ohmic relationship in the low-voltage region indicates the dominance of a thermally generated carrier density, rather than an injected carrier density. However, in the high-voltage region, the gradient of the $\log(I)-\log(V)$ plot was approximately 2, which indicates a predominance of SCLC current flow without traps. It should be noted that the observation of SCLC current, which was observed up to the RESET voltage without degradation, implies that bi-stable switching results in an interface effect, with the formation of non-metallic CFs.[3] Moreover, based on first-principle calculations, a distribution of isolated V_O is expected, as opposed to the formation of V_O clusters.[19,20] Thus, isolated V_O centers can remain in a TMO system and provide the conduction pathways.[19] At the BRS driving voltage in the 10% Hf:NiO_x devices, CFs may transform to non-negligible traps, such as V_O. In this case, the VCM with interface effects is the most appropriate model to explain this transition BRS mode (Fig. 3(b)). At the initial NHRS state, because of the thick interface-insulating layer that forms in the highly stoichiometric system, the NHRS is maintained. However, when the applied voltage reaches the negative SET voltage, current can flow in the NLRS through V_O based CFs, with the oxygen ions migrating to the Pt electrode, which moderates the interface oxide layer. In contrast to the URS mode, and despite applying a higher voltage, the RESET process did not occur because the formed filaments were not thick and dense enough to generate the heat required for rupturing them. For RESET to occur, the opposite polarity of the applied voltage is required. When the applied voltage reached the positive RESET bias, where the migrated oxygen forms an interface-insulating layer again at the Al electrode, it can switch to the PHRS and complete the 1 cycle of RRAM operation. In this case, the role of left-behind oxygen vacancies is not critical due to the interface insulating oxide layer.

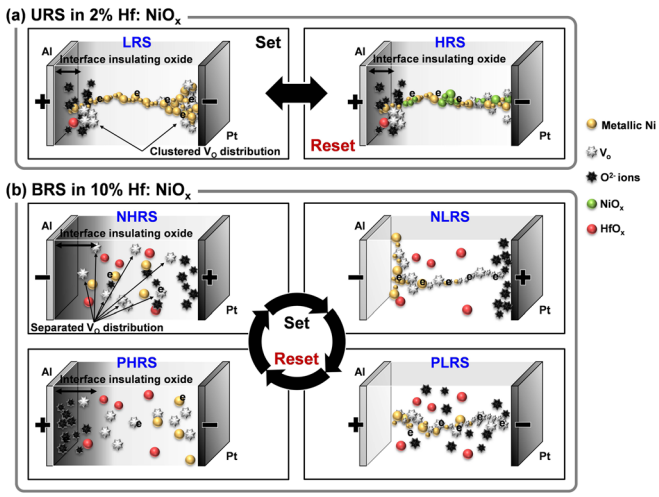

FIG. 3. (a) TCM model describes the behavior of the 2% Hf:NiO_x. The bi-stable URS mode is based on oxidation and reduction of the metallic Ni component. (b) VCM model describes the behavior of the 10% Hf:NiO_x. An interface insulating oxide layer and separated V_O centers can explain the BRS mode.

Figures 4(a) and 4(b) show cross-sectional high-resolution transmission electron microscopy (HR-TEM) images of the 2% and 10% Hf:NiO_x device, respectively. In both cases, interface oxides were observed; however, the thickness for this layer was 3.78 nm in the 2% device and 7.52 nm in the 10% device. The extended high-resolution image of the 2% in Fig. 4(c) reveals well-defined nanocrystalline grains with a d-spacing of 2.444 Å, 2.079 Å, and 1.476 Å. A fast Fourier transform (FFT) was applied to the image (inset of

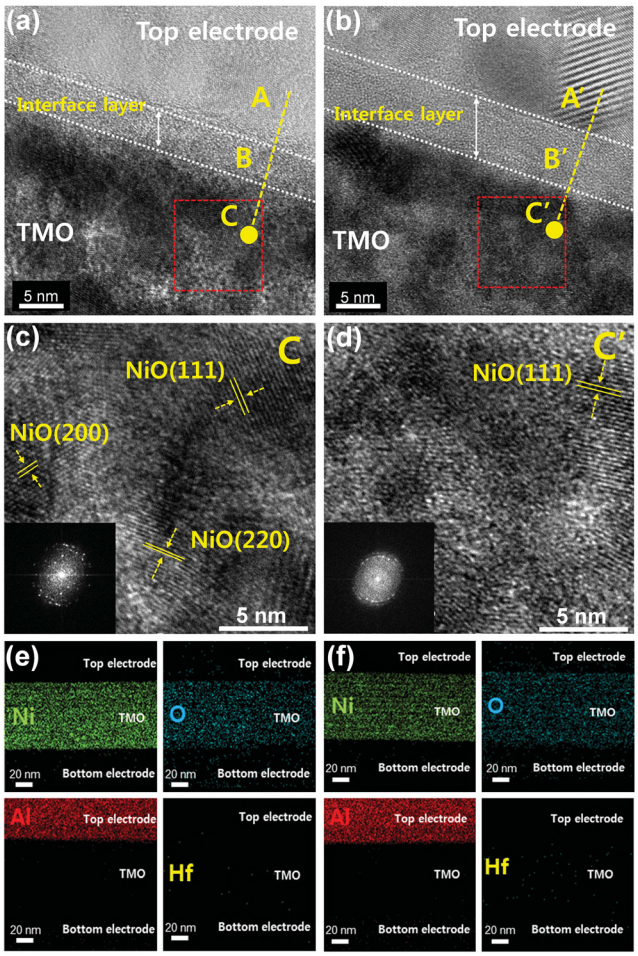

FIG. 4. The cross-sectional HR-TEM images of (a) 2% and (b) 10% Hf:NiO_x based RRAM. In common, the top electrode (A and A′), interface layer (B and B′), and TMO (C and C′) are depicted. The extended HR images of 2% and 10% Hf:NiO_x layers are shown in (c) and (d), respectively. EDS mapping data were depicted at (e) 2% and (f) 10% Hf:NiO_x.

Fig. 4(c)), which confirms the nanocrystalline phases of the TMO layer in the 2% device. However, the extended HR-TEM image for the 10% device (shown in Fig. 4(d)) exhibited a broadened amorphous matrix. Energy dispersive spectroscopy (EDS) mapping shown in Figs. 4(e) and 4(f), together with a spot analysis (data not shown), confirmed the composition of the spots labeled A, B, and C in the figures to be Al, Al_2O_3, and Hf:NiO_x, respectively. Interestingly, although there was almost no Al detected in spot C (the 2% device, Fig. 4(c)), a significant amount of Al was detected in spot C′ (the 10% device, Fig. 4(d)). This can be understood by considering the high negative SEP of Hf compared with that of Ni. In fact, by the line scan of EDS profile spot A to C (Fig. 5(a)) and A′ to C′ (Fig. 5(b)), Al related oxide layer can be detected with more quantitative way. It is apparent that the thicker interface oxide is expected and originated from the higher Hf concentration. Thus, it seems that the thicker interface oxide with potential Al distribution at TMO layer performed crucial role for the transformation of driving mode, URS to BRS. Specifically, in 10% Hf:NiO_x system, the segregated ions are not likely to form CF and control resistive switching behavior.[6–9] Rather, they are associated with the nonmetallic behavior as a result of oxidation, which leads to weaker and thinner CFs. In this case, the current in

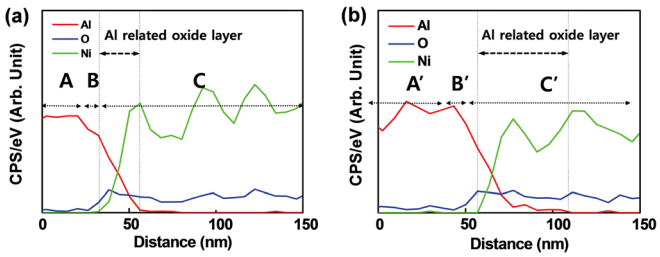

FIG. 5. EDS profiles at the interface region of the (a) 2% and (b) 10% Hf structures.

TABLE I. Calculated integration O 1s composition of Gaussian subpeaks.

E_B (eV)	O^{2-} related (527–530 eV)	O^- related (530.6–531.1 eV)	OH^- related (531.1–532 eV)
Hf:NiO_x (2%)	74.1%	11.5%	14.3%
Hf:NiO_x (10%)	76.9%	14.0%	9.0%
Hf:NiO_x (30%)	76.8%	18.4%	4.6%
Hf:NiO_x (100%)	82.5%	13.0%	4.2%

the structure is attributed to electron hopping between V_O sites.[10–12] X-ray photoelectron spectroscopy (XPS) was used to characterize the Hf content in the NiO_x system. The O 1 s peaks corresponding to 2%, 10%, 30%, and 100% Hf:NiO_x fitted using Gaussian subpeaks centered at 529.34 eV, 530.97 eV, and 532.09 eV (see supplementary material for Figure S2[24]). Each subpeak represents the lattice oxygen, V_O, and hydroxide-related component, respectively.[21] The composition are summarized in Table I. The most prominent feature of the O 1s spectra is an increase of the lattice oxygen peak following the increased Hf content. This behavior suggests that the incorporated Hf acts as an oxygen supplier at any concentration. However, it is worth noting that the fraction of V_O increased when the Hf concentration was increased from 2% to 30%, even though the overall non-lattice concentration decreased. This suggests that the Hf also acts as defect creator via a reduced E_v^f up to 30% Hf incorporation. Also, the increased concentration of V_O in the range of 2% to 10% Hf:NiO_x indicates that the V_O centers may facilitate the formation of CFs. Moreover, the generation of V_O centers is enabled by lowering E_v^f near the Hf doped sites.[10–12] The V_O centers can form a non-metallic filament network in the LRS of the 10% Hf. The measurements on Ni 2p XPS spectra also support abovementioned aspects (see supplementary material for Figure S3[24]).The peak centered at 853.7 eV indicates a metallic Ni component,[22] and as the Hf content increased, this metallic Ni peak shifted to higher energies, broadened, and eventually became indistinguishable from the shoulder peak that originates from NiO[23] at Hf fractions above 30%. These results are consistent with the non-stable phenomena related to diminished metallic Ni levels.[6]

In summary, we researched the Hf incorporation effect which accompanies the variation of resistive switching characteristics on solution-processed NiO_x based RRAM. The varied Hf incorporation contents were 2%, 10%, 30%, and 100%, and each amount results in the differences among the resistive switching characteristics. At 2% Hf:NiO_x, bi-stable URS

mode was clearly shown, and unexpected transformation to bi-stable BRS was observed at the 10% Hf:NiO_x. At 30% and 100% Hf:NiO_x, un-stable BRS mode and non-stable dielectric breakdown were observed, respectively. The transition of driving mode URS to BRS is mainly attributed to the generation of thicker interface oxide layer and potential Al distribution at TMO layer with the V_O distribution effect. Also, the variation to bi-stable memory switching to un-stable resistive switching characteristics is mainly caused by the reduced metallic Ni components and the shrunken grain size. The extinction of metallic Ni, amorphized phase, and degradation of V_O concentration with highly stoichiometric system lead the non-stable dielectric breakdown.

This work was supported by the National Research Foundation of Korea (NRF) Grant funded by the Korean Ministry of Education, Science and Technology (MEST) [No. 2011-0028819].

[1]M.-J. Lee, C. B. Lee, D. Lee, S. R. Lee, M. Chang, J. H. Hur, Y.-B. Kim, C.-J. Kim, D. H. Seo, S. Seo, U.-I. Chung, I.-K. Yoo, and K. Kim, Nature Mater. **10**, 625 (2011).
[2]J.-S. Lee, J. Mater. Chem. **21**, 14097 (2011).
[3]R. Waser, R. Dittmann, G. Staikov, and K. Szot, Adv. Mater. **21**, 2632 (2009).
[4]R. Jung, M. J. Lee, S. Seo, D. C. Kim, G. S. Parks, K. Kim, S. Ahn, Y. Park, I. K. Yoo, J. S. Kim, and B. H. Park, Appl. Phys. Lett. **91**, 022112 (2007).
[5]R. Waser and M. Aono, Nat. Mater. **6**, 833 (2007).
[6]M. J. Lee, Y. Park, S. E. Ahn, B. S. Kang, C. B. Lee, K. H. Kim, W. X. Xianyu, I. K. Yoo, J. H. Lee, S. J. Chung, Y. H. Kim, C. S. Lee, K. N. Choi, and K. S. Chung, J. Appl. Phys. **103**, 013706 (2008).
[7]C.-Y. Liu, X.-J. Lin, H.-Y. Wang, and C.-H. Lai, Jpn. J. Appl. Phys., Part 1 **49**, 056507 (2010).
[8]J. Kim, K. Lee, and H. Sohn, J. Electrochem. Soc. **156**(12), H881 (2009).
[9]K. Jung, J. Choi, Y. Kim, H. Im, S. Seo, R. Jung, D. Kim, J.-S. Kim, B. H. Park, and J. P. Hong, J. Appl. Phys. **103**, 034504 (2008).
[10]H. Zhang, B. Gao, B. Sun, G. Chen, L. Zeng, L. Liu, X. Liu, J. Lu, R. Han, J. Kang, and B. Yu, Appl. Phys. Lett. **96**, 123502 (2010).
[11]H. Zhang, L. Liu, B. Gao, Y. Qiu, X. Liu, J. Lu, R. Han, J. Kang, and N. Yu, Appl. Phys. Lett. **98**, 042105 (2011).
[12]M. S. Lee, S. Choi, C.-H. An, and H. Kim, Appl. Phys. Lett. **100**, 143504 (2012).
[13]D. H. Yoon, S. J. Kim, J. Jung, H. S. Lim, and H. J. Kim, J. Mater. Chem **22**, 34 (2012).
[14]S. H. Chang, J. S. Lee, S. C. Chae, S. B. Lee, C. Liu, B. Kahng, D.-W. Kim, and T. W. Noh, Phys. Rev. Lett. **102**, 026801 (2009).
[15]I. Hwang, M.-J. Lee, G.-H. Buh, J. Bae, J. Choi, J.-S. Kim, S. Hong, Y. S. Kim, I.-S. Byun, S.-W. Lee, S.-E. Ahn, B. S. Kang, S.-O. Kang, and B. H. Park, Appl. Phys. Lett. **97**, 052106 (2010).
[16]S. Lee, H. Kim, J. Park, and K. Yong, J. Appl. Phys. **108**, 076101 (2010).
[17]W. J. Park, H. S. Shin, B. D. Ahn, G. H. Kim, S. M. Lee, K. H. Kim, and H. J. Kim, Appl. Phys. Lett. **93**, 083508 (2008).
[18]J. W. Seo, J.-W. Park, K. S. Lim, J.-H. Yang, and S. J. Kang, Appl. Phys. Lett. **93**, 223505 (2008).
[19]B. Gao, J. Kang, B. Chen, P. Huang, L. Ma, F. Zhang, L. Liu, X. Liu, X. A. Tran, and H. Yu, in *2012 IEEE 11th International Conference on IEEE Solid-State and Intergrated Circuit Technology (ICSICT)* (IEEE, 2012), p. 6467605.
[20]H. D. Lee, B. Magyari-Kope, and Y. Nishi, Phys. Rev. B **81**, 193202 (2010).
[21]J.-C. Dupin, D. Gonbeau, P. Vinatier, and A. Levasseur, Phys. Chem. Chem. Phys. **2**, 1319 (2000).
[22]S. Uhlenbrock, C. Scharfschwerdt, M. Neumann, G. Illing, and F.-J. Freund, J. Phys. Condens. Matter **4**, 7973 (1992).
[23]J. Jung, D. L. Kim, S. H. Oh, and H. J. Kim, Sol. Energy Mater. Sol. Cells **102**, 103 (2012).
[24]See supplementary material at http://dx.doi.org/10.1063/1.4867233 for additional information.